Electronic Supplementary Information (ESI)

Achieving battery-level energy density by constructing aqueous carbonaceous supercapacitors with hierarchical porous N-rich carbon materials

5 **Mei Yang,† Yiren Zhong,† Jie Bao, Xianlong Zhou, Jinping Wei, Zhen Zhou***

Tianjin Key Laboratory of Metal and Molecule Based Material Chemistry, Key Laboratory of Advanced Energy Materials Chemistry (Ministry of Education), Institute of New Energy Material Chemistry, Collaborative Innovation
10 *Center of Chemical Science and Engineering (Tianjin), Nankai University, Tianjin 300071, China.*

Corresponding Author, E-mail: zhouzhen@nankai.edu.cn
† Both authors contributed equally to this work.

15

20

25

30

In a typical fabrication of symmetric supercapacitor devices, two current collectors (graphite paper, ~7.5 mg × 2), one piece of separator (cellulose paper, ~8.0 mg), external packaging (tape package, ~19.0 mg), acidic electrolytes (1 M H_2SO_4, ~30.0 mg), and electrodes (including active material, conductive agent, and binder; ~13.0 mg × 2) are assembled under certain pressure (Fig. S1).

5 In this manuscript, specific capacitances (C, F g⁻¹), energy density (E, Wh kg⁻¹) and power density (P, W kg⁻¹) were calculated through generally-adopted equations (*Adv. Mater* 2012, 24, 5713–5718).

$$C = \frac{It}{m\Delta V} \tag{1}$$

$$E = 0.5 C_T V^2 / 3.6 \tag{2}$$

$$P = 3600 \times E / \Delta t \tag{3}$$

10 where I (A), m (g), and t (s) denote discharge current, mass of active materials, and discharge time, respectively. C_T (F g⁻¹) represents the specific capacitance of supercapacitor cell and V (V) is the voltage change during the discharge process after internal resistance (IR) drop.

As for single-electrode performances in a three-electrode setup, we have considered the weight of total electrode materials including the active carbon material, conductive agent, and binder in the calculation.

15 For electrode-level performance of symmetric cells, C_T is calculated based on the total mass of both electrodes, including the active material, conductive agent and binder. For device-level performance, the values are calcultated based on the weight and volume of total package devices into account, including the current collector, seperator, electrolyte, external packaging and etc.
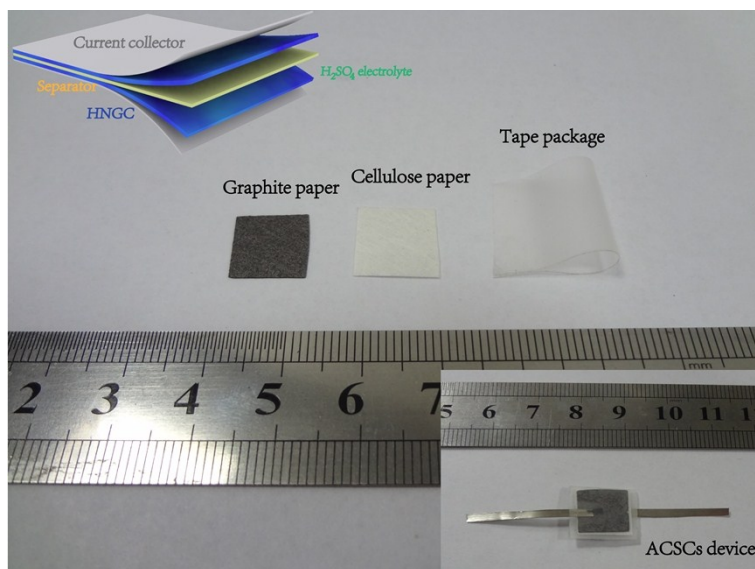

20

Figure S1 Digital photos of the aqueous carbonaceous supercapacitors (ACSCs) device.

Table S1. Porous properties of micro-NGC, meso-NGC materials, HNGC-X (X= 750, 850, and 950), and reference AC.

Samples	BET Surface Area (m²/g)	External Surface Area (m²/g)	Micropore Area (m²/g)	Pore Volume (cm³/g)	Elemental Analysis (wt%)		
					C	N	H
micro-NGC	593.03	166.53	426.50	0.919	75.35	11.47	3.51
meso-NGC	440.40	381.4	59.0	1.366	76.28	10.91	4.39
HNGC-750	322.9	226.6	96.30	1.488	73.66	13.75	3.94
HNGC-850	409.15	301.43	107.73	1.663	75.69	10.77	4.17
HNGC-950	477.45	308.76	168.69	1.735	85.79	6.40	2.39
AC	2116.07	362.25	1753.82	1.105	92.89	-	1.99
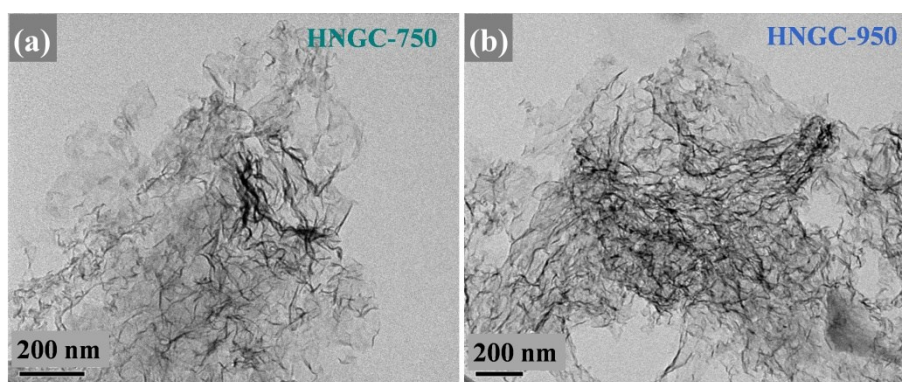
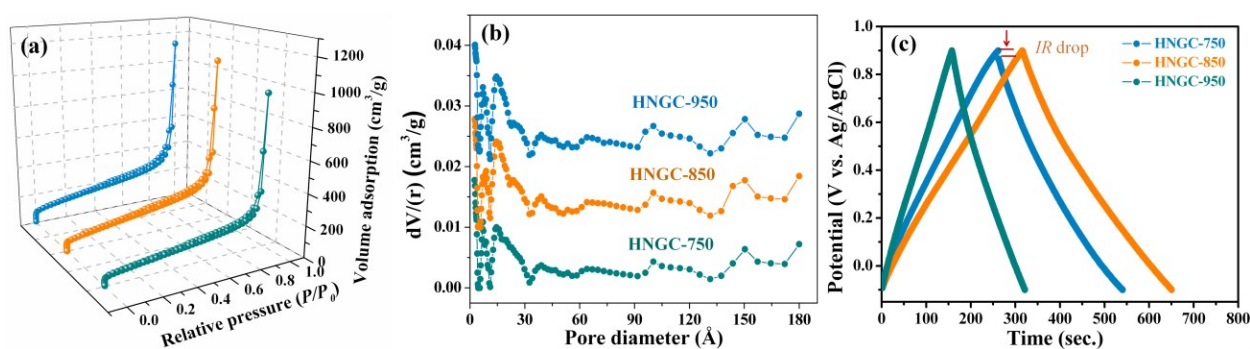5   **Figure S2** TEM images of HNGC-750 (a) and HNGC-950 (b).

Figure S3 Nitrogen adsorption-desorption isotherms of HNGC-X (a), and corresponding pore-size distribution (b); Galvanostatic charge/discharge curves (c) of HNGC-X at a current density of 2 A g⁻¹.
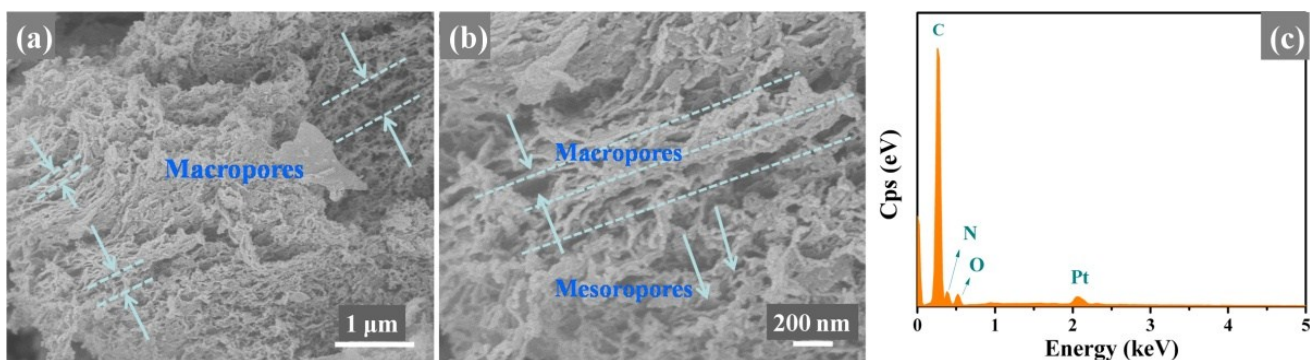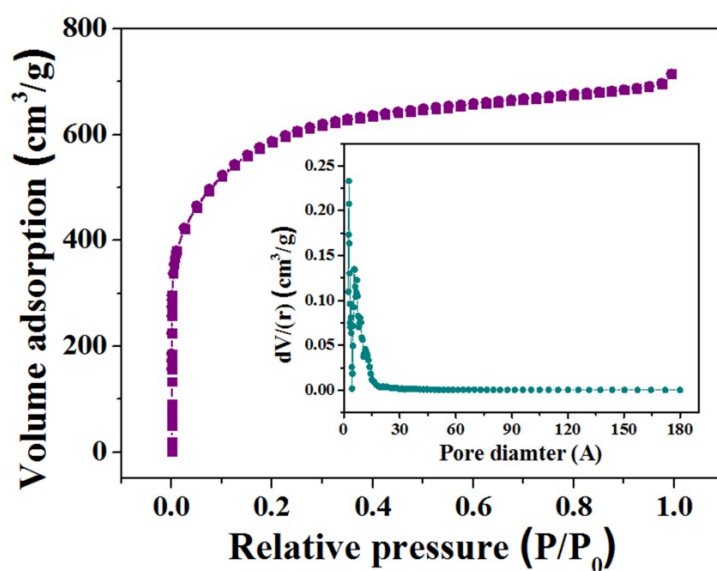
Figure S4 (a, b) SEM images and (c) EDS of HNGC.

5 **Figure S5** Nitrogen adsorption-desorption isotherms of AC, and inset shows corresponding pore-size distribution.
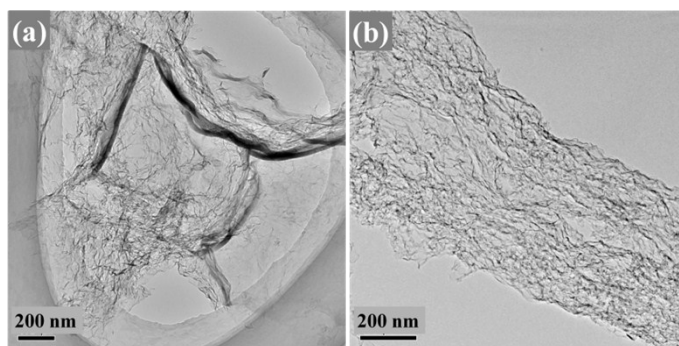

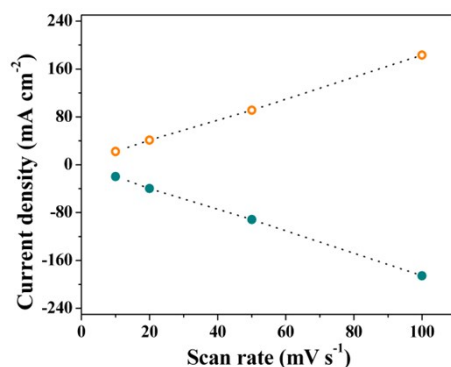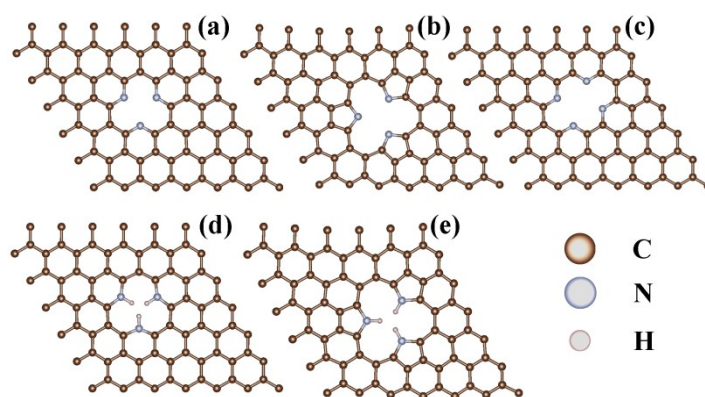**Figure S6** TEM images of micro-NGC (a) and meso-NGC (b).

Figure S7 The linear relationship between current densities and scan rates.

5 **Figure S8** Geometry configurations of pyridinic defected graphene (a), pyrrolic graphene (b), pyridinic graphene with larger hole size (c), hydrogenated pyridnic graphene with three H (d) and hydrogenated pyrrolic graphene with three H (e) with all the vacuum layers of 20 Å. The colors associated with the represented atoms are shown at last. The hole sizes, which are defined here as the distance from the hole center to the N atom, in (a), (b) and (c) are 1.52 Å, 1.70 Å and 1.91 Å, 10 respectively.

Computational Details

Pyridinic (Fig. S8a) and pyrrolic (Fig. S8b) nitrogen-containing defects in 2D graphene networks were modeled. To compare the difference in their ability to attract protons, another pyridinic-N graphene with larger hole size (Fig. S8c) 15 was also modeled to identify the influence of defect sizes. The following reactions were first considered: $H_{x-1}NGC + H^+ + e^- \rightarrow H_xNGC$, where $H_{x-1}NGC$ and H_xNGC represent the pyridinic/pyrrolic-N graphene with a number of x-1 and x H atoms attached to it, respectively. Similar to the computations in lithium ion batteries, $H^+ + e^-$ are replaced by $1/2\ H_2$ (*J. Phys. Chem. B*, 2004, 108, 17886-17892).

Practically ion mobility is defined by activation energy computed by NEB; while in this situation, the reactions that protons adsorbed by HNGC go through continuous energy decrease, meaning that there are no energy barriers. For a certain reaction, the energy change (dE) is resulted from the multiples of the intermolecular interaction (F_{ij}) and the distance (dl), and such relationship can be described as following:

5
$$dE = \int F_{ij} \cdot dl \tag{4}$$

This formula suggests that we can get the interaction of two species by differentiating the energy change. Given that such interaction is in form of force, then we can tell the differences of the acceleration. For a large quantity of static atoms which are supposed to be static at the beginning, we will be able to estimate the average velocity during a certain path.

10   In our work, we posed protons at different distances from the carbon sheet (without further optimization because we are only interested in the energy change resulting from the distance change) and drew the energy-distance curve. If, we expected, a certain path went through a higher rate of energy descend (RED), we could say that protons were under more attraction of that carbon sheet. With this conception, we studied such energy-distance curves of four structures, the first three of which are graphene, pyridinic and pyrolic defects, and the last of which is another

15 pyridinic defects with a larger hole (Fig. S8c). Note that protons move in a path vertical to HNGC, 10 Å to 2 Å from them, and the extended lines of the path cross the center of the defects.

Table S2. Physical properties and capacitances of the HNGC and AC electrodes at a current density of

20 2 A g^{-1}.

Samples	Tap density (g cm^{-3})	Packing density (g cm^{-3})	Gravimetric capacitance (F g^{-1})	Volumetric capacitance (F cm^{-3})
HNGC	0.33	0.93	710	646
AC	0.38	0.58	183	101

As electrode materials, the tap density (ρ_{tap}) and electrode-packing density ($\rho_{packing}$) play significant roles of supercapacitors. Particularly, $\rho_{packing}$ is directly related to the electrochemical performance of whole devices (volumetric capacitance based on real devices). Herein, we explored both tap density and electrode-packing density.

25 The ρ_{tap} was measured by 6000-time vibration in tapping apparatus, and $\rho_{packing}$ was measured according to the formula,

$$\rho = m / Sd \tag{5}$$

Where m is the mass of dried carbon materials (g), S and d are the area (cm^2) and thickness (cm) of the effective carbon electrode, respectively.
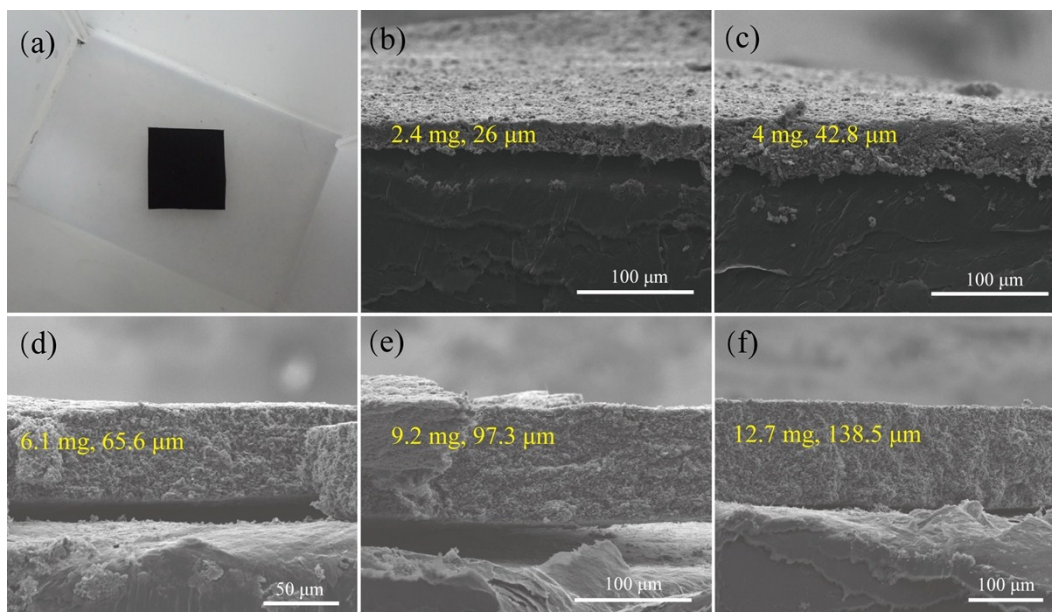
30

Figure S9 Cross-section SEM images of the HNGC electrodes with different mass loadings.

In order to understand the effect of mass loading, the relationship between mass loading and initial capacitance was
5 further studied, wherein the detailed contrast is shown in Fig. S9. At a current density of 2 A g^{-1}, the performance of
1.1 mg/cm^2 loading reaches an initial capacitance up to 705 F g^{-1}. When the mass loading ranges from 3 to 15 mg/cm^2,
small capacitance difference (610 to 660 F g^{-1}) can be observed. Note that an obvious drop of capacitance to 522 F g^{-1}
is detected once the loading approaches 20 mg/cm^2. This phenomenon is mainly due to the shorter ion transport path
and better utilization of active materials at low mass loading, while large region of insufficient electrode-electrolyte
10 contact at larger mass loading. It is proved by Cui group (*ACS Nano*, 2011, 5, 8904-8913) that at a fixed scan rate, the
areal capacitance increases with electrode material thickness or mass until a critical value is reached. Moreover, such
high capacitance retention even at 15 mg/cm^2 further testifies beneficial effects of the hierarchical porous structure on
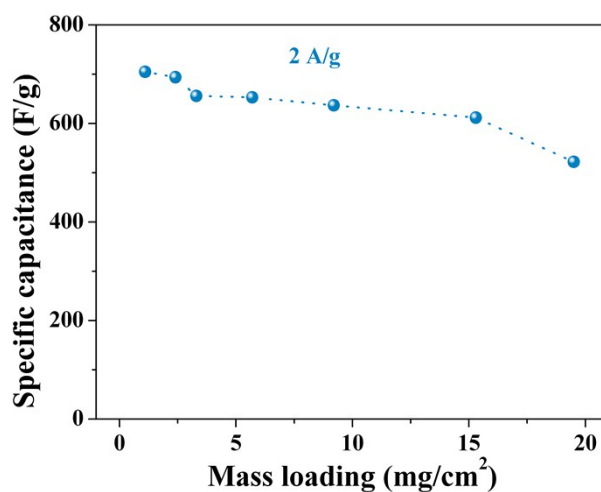ion transport.

15 **Figure S10** Specific capacitance with respect to   the amount of mass loading.
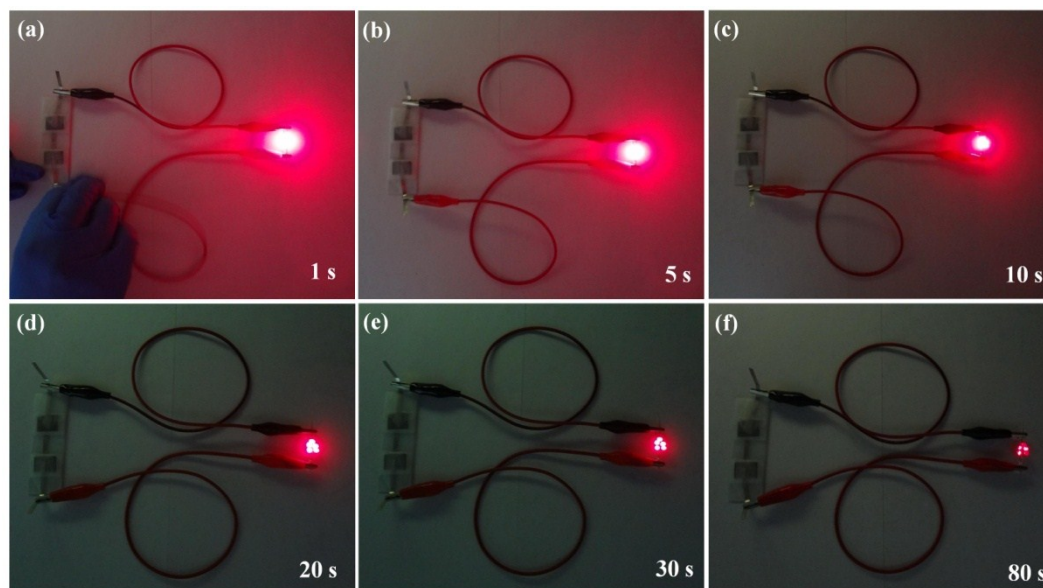
ARTICLE TYPE

Figure S11 (a-f) Five LED indicators powered by two ACSCs in series and detailed brightness changes with time after charging for short 30 seconds.

5